Journal of Magnetic Resonance 380 (2025) 107953

Contents lists available at ScienceDirect

Journal of Magnetic Resonance

journal homepage: www.elsevier.com/locate/jmr

Specificity and reactivity of bromoacrylaldehyde spin labels

Dominik Gendreizig [a,1], Christina Elsner [a,1], Svetlana Kucher [a], Gunnar Jeschke [b], Alistair J. Fielding [c,*], Enrica Bordignon [a,*]

[a] Department of Physical Chemistry, Sciences II, University of Geneva, 30 Quai Ernest Ansermet, 1211 Geneva, Switzerland
[b] Institute of Molecular Physical Science, ETH Zurich, Vladimir-Prelog-Weg 1-5/10, CH-8093 Zurich, Switzerland
[c] Centre for Natural Products Discovery, James Parsons Building, Liverpool John Moores University, Byrom Street, Liverpool L3 3AF, United Kingdom

A B S T R A C T

Electron paramagnetic resonance (EPR) spectroscopy in combination with site-directed spin labelling provides information on structure and dynamics of biomolecules. Increasing the availability of spin labels with different properties is an elegant way to foster a more accurate analysis of the EPR data in relation to the biological problem investigated. In this study, we present a comparative investigation of labelling efficiency, surface accessibility, site specificity and width of the distance distributions obtained on two proteins with the nitroxide-based bromoacrylaldehyde spin label (BASL) versus the two commercial spin labels MTSL (methanethiosulfonate spin label) and MAP (maleimido proxyl). Based on the predicted distances from a rotamer library approach and on the experimental distance distributions, BASL is shown to provide generally narrower distance distributions compared to the other nitroxide labels. The exquisite surface specificity of BASL with respect to MAP could be successfully exploited to selectively label surface cysteines in proteins containing a high number of native cysteines. In addition, the distinct site-reactivity of BASL and MAP towards two surface-exposed cysteines was leveraged for orthogonal labelling strategies with nitroxide and gadolinium labels.

1. Introduction

Site-directed spin labelling (SDSL) [1] has enabled a wide range of proteins of different sizes to be studied in aqueous and membrane environments using electron paramagnetic resonance (EPR) spectroscopic techniques [2–4]. Several spin labels were developed to probe specific structural and dynamic properties of biomolecules using continuous-wave (cw) EPR and pulse EPR techniques, of which the most commonly used is Double Electron-Electron Resonance (DEER, also known as PELDOR) [1,5–7]. Nitroxide labels were the first to be introduced to study proteins' dynamics and structural changes [8–10] *in vitro*, however, a series of alternative labels were synthesized and characterized in the last decade to overcome chemical reduction in reducing or cellular milieu and/or additionally offer a higher sensitivity in pulsed EPR, e.g. sterically-shielded nitroxides [11–13], triarylmethyl-based radicals [14,15], gadolinium-based labels [16,17], Cu(II)-based labels [18–20], etc.

The availability of several spectroscopically distinct labels has been also further explored to increase the information content per sample using orthogonal labelling strategies, especially with pulsed dipolar methods [6,21–23].

Despite the large array of different labels' types, nitroxide labels have key advantages: i) a relatively small size, which minimizes the risk of disrupting the native structure and ii) the ability to be excellent reporters of both rotational dynamics at physiological temperatures and interspin distances at cryogenic temperatures [8]. One main disadvantage is the chemical reduction of the NO group in presence of reducing agents present in cellular milieu, which can be in any case partially overcome by chemical modification of the labels. Among the nitroxide labels, the methanethiosulfonate nitroxide (MTSL) [10], attached to a cysteine residue via a disulfide linkage, is still the label of choice for most proteins in non-reducing environments. MTSL is highly selective for cysteine residues, with well-documented rotamer libraries [24,25] and internal side chain dynamics [26–29].

MTSL is highly reactive towards surface cysteines and the modified side chains are less likely to perturb structure. In these favourable cases it is easier to correctly predict the populated rotamers, allowing more accurate simulations of interspin distance distributions [2]. However, MTSL was early recognized to be able to attach to cysteines which are partially solvent-accessible or located in transmembrane helices (see for example [30,31]). Therefore, the use of MTSL usually requires the removal of at least some native cysteines in the proteins under investigation. Depending on the sites chosen and the conformational freedom of the system, the existence of multiple rotamers can lead to overly

* Corresponding authors.
E-mail addresses: A.J.Fielding@ljmu.ac.uk (A.J. Fielding), enrica.bordignon@unige.ch (E. Bordignon).
[1] shared first authorship

https://doi.org/10.1016/j.jmr.2025.107953
Received 14 May 2025; Received in revised form 7 August 2025; Accepted 11 August 2025
Available online 12 August 2025

broad distance distributions, which generally reduces the accuracy of distance constraints for coarse-grained modelling of conformational changes of proteins.

To overcome the complexities associated with the flexibility of MTSL, a range of more rigid spin label nitroxides have been developed. For example, the 4-pyridyl substituted spin label of MTSL gives rise to a side chain that has been shown to have a considerable reduction in the flexibility when in a solvent exposed α-helix [32]. A bi-functional analogue of MTSL, RX3 [33], tethers to two cysteines, simplifying rotamer dynamics interpretation and producing narrower distance distributions, however the cysteines must be specifically introduced at i and $i + 3/4$ positions in an α-helix or at i and $i + 1$ in a β strand, which might limit its broad application. Another commercially available nitroxide label is the maleimide-proxyl (MAP) [34], which is slightly bulkier than MTSL and is attached to the cysteine via an irreversible C—S bond, which can be favourable in particular conditions (e.g. crowded protein environment with cys-containing proteins). MAP was found to produce a monomodal distance distribution compared to a bimodal distribution obtained with MTSL attached to the same sites on a immunoglobulin-binding domain [35].

Proteins with a higher natural cysteine content remain challenging for most cys-targeting labels, especially if it is not possible to remove key natural cysteines in the protein without affecting its structure or function. While insertion of unnatural amino acids and subsequent labelling could be an option in those cases [36–38], it would be beneficial to have surface-specific labels targeting cysteines, allowing for a more optimized SDSL-approach adapting to the systems at hand while minimizing the genetic modifications. It is therefore important to continue exploring the chemical scope of cys-targeting nitroxides to improve the armoury of labels for a greater range of protein systems.

The nitroxide studied in this work is the bromoacrylaldehyde spin label (BASL, CAS 85591–99-7) [39,40], attached with a three-bond tether to a cysteine residue via a Michael-addition at basic pH. BASL showcased surface selectivity and rigid dynamics on a model system. DEER distance distributions and modulation depths were similar to those of MTSL; however, the limited range of protein examples and the absence of a supporting rotamer library have restricted its broader application.

Other spin label chains attached to proteins via a thioether [41–43] have been also employed featuring very rigid labels such as the label InVSL [44]. The same chemical methodology was employed to attach the methyl 4-fluoro-2,2,5,5-tetramethyl-2,5-dihydro-1H-pyrrole-3-carboxylate-1-yloxyl radical with a three bond tether to cysteine residues in T4-lysozyme variants [45]. This approach proved valuable for monitoring slow internal structural fluctuations and was also effective for distance mapping using dipolar spectroscopy and relaxation enhancement techniques. Additional advantages of the three-bond tether approach and its overall small size may include reduced steric interference with protein folding and binding partners.

In this work we present the rotamer library for BASL implemented in MMM software [46,47] and compare the performance of BASL, MTSL and MAP to highlight differences and advantages of each spin labelling strategy to maximize informational gain for proteins. As model systems, two water soluble proteins were selected whose structure is known: mouse Bid (PDB: 1DDB) [48], a proapoptotic protein of the Bcl-2 family known to induce death receptor-mediated apoptosis and γD-crystallin (PDB: 1HK0, called crystallin in the following for simplicity) [49], one of the most abundant proteins in the nucleus of the human lens.

Here, we demonstrate that the rotamer library predicts well the experimental distances measured by DEER on two BASL-labelled proteins. BASL's unique properties did not only cause comparatively narrower distance distributions than MTSL but its surface- and site-specificity opened the possibility to specifically label proteins with a higher number of natural cysteines and to apply orthogonal labelling strategies.

2. Materials and methods

2.1. Sample preparation

2.1.1. Bid

His-tagged mouse Bid was expressed in the pET23d-vector [50] in *E. coli* with 1 mM IPTG. Briefly the recombinant protein was purified from the soluble fraction of the bacterial lysate using Ni-NTA beads (*Ni-NTA Superflow* by *Qiagen*). It was first washed without imidazole (20 mM Tris, pH 7.5, 20 mM NaH_2PO_4, 300 mM NaCl) followed by washing steps with 10 mM and 25 mM imidazole, respectively. After elution with 250 mM imidazole, the protein was dialyzed and stored in 20 mM Tris (pH 7.5) and 150 mM NaCl.

Before labelling, Bid (containing two native cysteines C30 and C126) was incubated 1 h with 1 mM DTT. DTT was removed with a desalting column and the labelling reaction was performed in labelling buffer (20 mM Tris (BASL: pH 8.3, MAP: pH 7.5), 150 mM NaCl) with 1:30 protein-to-BASL or 1:10 protein-to-MAP overnight at 8 °C. The residual free label was removed using desalting columns. The protein was concentrated to the final concentration using 10 kDa-cutoff centricons (Amicon). The final concentration was determined via absorbance at 280 nm ($\varepsilon = 8490\ M^{-1}\ cm^{-1}$).

2.1.2. γD-crystallin

γD-crystallin variants were prepared as previously described [51]. For spin labelling, γD-crystallin variants (wild type, S73C and C111S-S73C) were incubated with 1 mM DTT for 1 h at room temperature. Labelling with BASL was shown not to affect the ability of crystallin to undergo liquid-liquid phase separation (Fig. S1). DTT was removed by a PD-10 desalting column equilibrated with Tris buffer solution (20 mM Tris, 150 mM NaCl, pH 7.5). BASL and MAP (Sigma Aldrich) were added to the wild type and the C111S-S73C variant in a 1:1.2 ratio protein-to-label at pH 7.5 (called 1:1 for simplicity in the text), while the variant S73C was incubated with BASL, MAP and MTSL in a 1:2.2 (called 1:2) protein-to-label ratio at pH 7.5 (for labelling tests at pH 8.3 see Fig. S2). Labelling protocols with higher label-to-protein ratios were also used, as described in the appropriate legends. The samples were incubated overnight at room temperature and in the dark under constant shaking. Excess label was removed via PD-10 desalting column. The proteins were concentrated via Vivaspin 20 columns with a 10 kDa cutoff and the final concentration was determined via absorbance at 280 nm ($\varepsilon = 42{,}860\ M^{-1}\ cm^{-1}$).

For the orthogonal labelling, S73C was incubated for 1 h at room temperature with 1 mM DTT. DTT was subsequently removed via PD-10 column equilibrated with Tris buffer solution (pH 7.5). First MAP or BASL were added in a 1:1.2 ratio protein-to-label and incubated at RT in the dark under constant shaking for 8 h, excess label was removed via PD-10 column. Gd-DOTA maleimide was then added in a 1:1.2 ratio and incubated overnight under the same conditions. Excess label was removed via PD-10 column.

2.2. CW EPR measurements

All cw EPR experiments were performed on a Bruker E500 X-band (9.1–9.8 GHz frequency range) equipped with a super high Q cavity ER 4122 SHQ. The power was set to 2 mW and modulation amplitude to 0.1 mT. Samples (20 μL) were inserted into 50 μL glass capillaries (BLAUBRAND). The labelling efficiency of each protein variant was determined via comparison with a standard of 100 μM TEMPOL in water by double integration of the X-band EPR spectrum using the free software spintoolbox (https://www.spintoolbox.com/en/).

2.3. DEER measurements

DEER samples (40 μL) were inserted in 3.0 mm o.d. quartz tubes (Aachener Quarzglas) and flash frozen in liquid nitrogen. All samples

contained 50 % *v/v* fully deuterated glycerol (Sigma Aldrich) as cryoprotectant.

The pulse EPR experiments were performed on a Bruker Q-band (33.5–34.5 GHz) Elexsys E580 spectrometer equipped with a 150 W TWT amplifier and a Bruker Spinjet-AWG at 50 K for nitroxide-nitroxide (NO-NO) DEER and at 10 K for gadolinium-gadolinium (Gd—Gd) and nitroxide-gadolinium (NO-Gd) DEER. A homemade probe head [52] accommodating 3 mm o.d. tubes was used. As standard setup we used the dead-time free 4-pulse DEER sequence with Gaussian pulses [53] with 16-step phase cycling [54]. All pulses were set up to the same length (32–34 ns corresponding to 16–20 ns FWHM). For NO-NO DEER, the pump frequency was positioned at the maximum of the nitroxide spectrum and the observer at −90 or − 100 MHz depending on the resonator dip. For the Gd—Gd DEER, the pump frequency was set to the maximum of the gadolinium spectrum and the observer at −100 MHz. For the NO-Gd DEER, the pump frequency was set to the maximum of the nitroxide spectrum, while the observer frequency at −300 MHz (maximum of the Gd spectrum). The DEER parameters are shown in Table 1. The DEER traces were analyzed with DeerAnalysis 2022 (https://epr.ethz.ch/software.html) [55] using the user-unbiased neural network method DEERNet [56,57] according to the guidelines [58].

2.4. Rotamer library

A preliminary geometry of the construct shown in Fig. 1A, with the neighboring residues replaced by hydrogen atoms and the N—O group substituted by a C═O group, was generated with ChemDraw and Chem3D software and optimized with the MMFF94 forcefield. After replacing the carbon atom of the C═O group by nitrogen, this construct was geometry optimized in ORCA 5.0 [59] at UB3LYP/def2-SVP level. An ensemble of 50,000 conformers was generated by Monte-Carlo sampling of the four torsion angles indicated in Fig. 1A based on the UFF force field [60]. We oversampled the six canonical rotamers (Fig. 1B) by generating a library of 240 rotamers following an earlier approach [61] without softening the van-der-Waals potentials.

2.5. Structures and simulated distance distribution

For Bid, the 20 NMR models present in the PDB:1DDB were used. For crystallin, 20 or 80 snapshot structures were randomly extracted from the MD trajectories previously calculated on the single crystallin protein in the simulation box at 273 K [51] and compared to the available X-ray structure (PDB: 1HK0) in MMM [46]. The 80 snapshots were randomly taken at discrete time points within the 5 μs trajectory to perform the rotamer analysis and 20 snapshots were randomly selected from the 80 snapshots available to simulate the ensemble interspin distances. Rotamers and interspin distances were calculated on the snapshots of the MD trajectories or on the available PDB files using the software MMM version 2020.1 for MTSSL and MAP and 2023.3 for BASL (298 K libraries) [24,46,47]. Distance distributions for the whole MD trajectory of crystallin were also calculated using the software package DEERPREdict (https://github.com/KULL-Centre/DEERpredict) for the newly implemented MMMx libraries of MTSSL, MAP and BASL with the default parameters set at 273 K [62]. A comparison of the performance of the three libraries on the PDB:1HK0 using MMM or DEERPREdict can be found in Fig. S3.

Table 1
DEER setup parameters.

	NO-NO	Gd-Gd	NO-Gd
Temperature [K]	50	10	10
Shot repetition time [ms]	5	5	5
t_1 [ns]	400	800	800
t_2 [ns]	3000–5000	3800–4000	3800–4000
Zero time [ns]	120	520	520
t_1 averages in steps of 16 ns	8	8	8

3. Results

3.1. Rotational dynamics of BASL

The rotameric states accessible to BASL were assessed by the rotamer library analysis. The label features only three rotatable bonds between the peptide backbone and the nitroxide group (Fig. 1A). A fourth torsional degree of freedom arises for the aldehyde group attached to the nitroxide heterocycle. We find that the short linker considerably restrains rotamer distributions due to steric clashes. Whereas the distribution of torsion angle χ_2 features three maxima for MTSL [24], only one of them is accessible for BASL (Fig. 1B). Likewise, only the trans conformation is populated with respect to torsion angle χ_4, since the aldehyde oxygen atom and the sulphur atom clash for the cis conformation. Therefore, BASL can be described by only six canonical rotamers, which allows for substantial oversampling of the conformation distribution by the rotamer library. Such oversampling is expected to improve accuracy of modelling. We decided on a rotamer library size of 240, which still enables fast computations.

Next, the spatial distribution of the unpaired electron with respect to the peptide backbone was studied for the case where the label does not interact with other amino acid residues. In Fig. 1C, the corresponding visualizations are compared for BASL (yellow), MTSL (teal), and MAP (red). The spatial distribution is more compact for BASL than for the other two labels. It is also more densely sampled by the rotamer library, although library size is similar for MTSL (216) and not much smaller for MAP (108). The distributions of the distance between the Cα atom and the midpoint of the N—O bond shown in Fig. 1D let us expect that BASL can provide narrower distance distributions that are closer to the Cα-Cα atom distance distribution for the spin-labelled pair of residues. This feature in turn should then reduce label-induced broadening [63] of modelled conformation ensembles of intrinsically disordered proteins.

To investigate the properties of MTSL, MAP and BASL attached to proteins, the two natural cysteines (30 and 126) of Bid and the two most exposed cysteines in crystallin (C111 and S73C) were labelled *in silico* with the rotamer libraries available in MMM [46,47] (Fig. 2). For both proteins there is an ensemble of structures to be considered for the rotamer analysis. For Bid, we considered the 20 available NMR models for *in silico* analysis and for crystallin we compared the available X-ray structure with the structural snapshots derived from a 5 μs MD trajectory of the protein at 273 K [51]. Using the ensemble models, the existing dynamics of the backbone and of the sidechains adjacent to the spin-labelled site can be partially considered within the rotamer analysis approach. As we will see later, the availability of structural ensembles facilitates the prediction of the actual accessibility of the labels in crystallin.

The analysis performed on Bid on the two natural cysteines with the three labels (Fig. 2A,B) shows that the number of rotamers on both sites is quite low in most models (less than 25), with BASL and MAP having lower numbers of rotamers with respect to MTSL (Fig. 2B). In both positions the root mean square deviation (rmsd) of the position of the NO radical scaled proportionally to the number of populated rotamers. For BASL, the highest rmsd observed (about 0.3 nm) is generally lower than that of the other two labels, in agreement with the more restricted internal dynamics of the label (Fig. 1).

The two surface-accessible cysteines (C111 and S73C) of crystallin (Fig. 2 C,D) showed a higher number of populated rotamers with respect to Bid, but interestingly, the root mean square deviation of the position of the NO group of BASL did not exceed the maximum value of about 0.3 nm even for >60 rotamers populated, indicating a more restricted localization of BASL with respect to MTSL and MAP (see also Fig. 1D). Notably, the structures of the ensemble have a large variability in terms of populated rotamers, which corroborate the notion that using ensemble structures from MD trajectories (or NMR models), provide

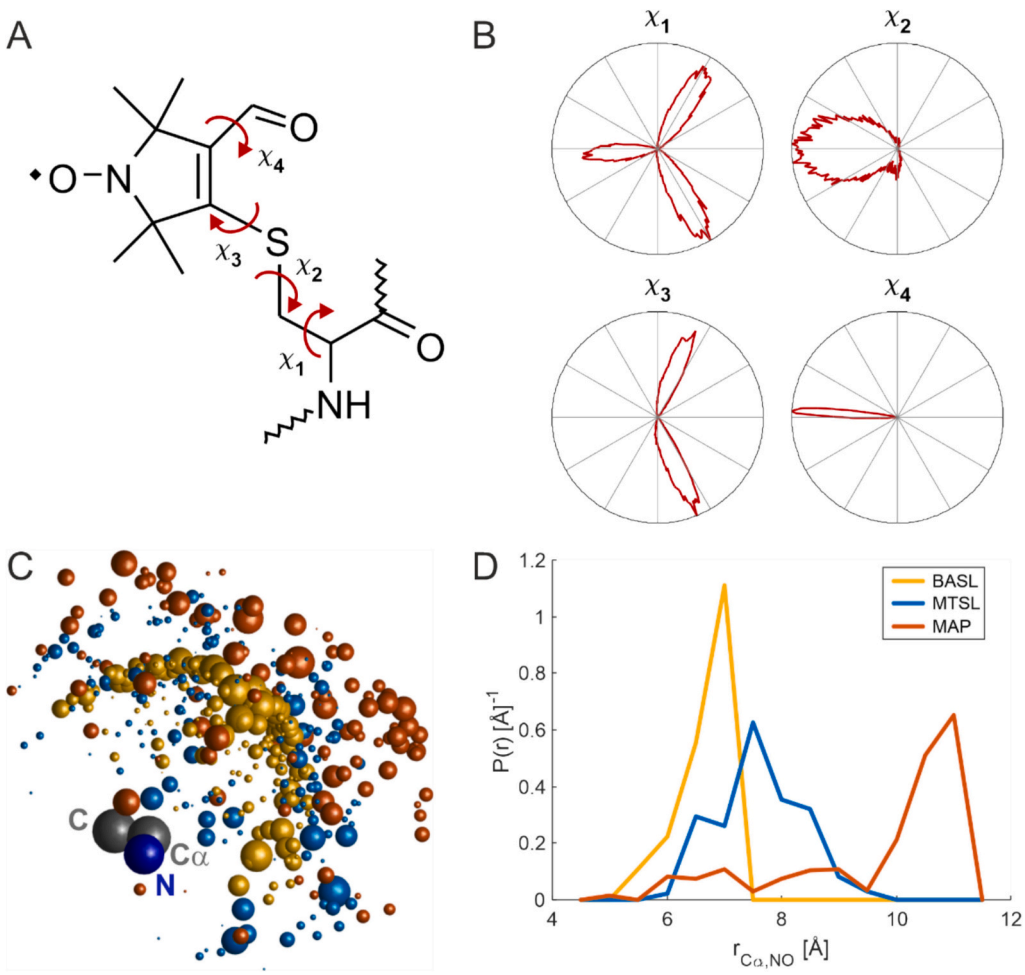

Fig. 1. Rotamer library for BASL and comparison to the MTSL and MAP libraries. A) Structure of BASL attached to the peptide backbone and definition of sidechain torsion angles χ_1-χ_4. B) Torsion angle distributions in an ensemble of 50,000 BASL sidechain conformers generated by a Monte Carlo procedure. C) Spatial distribution of the N—O bond midpoints with respect to the backbone atoms of the labelled residue for the MMM rotamer libraries of BASL (yellow), MTSL (teal), and MAP (red). Sphere volumes correspond to rotamer populations. The backbone atoms are displayed as larger spheres. D) Distributions of the distance between the Cα atom of the labelled residue and the N—O bond midpoint for the rotamer libraries of BASL (yellow), MTSL (teal), and MAP (red), disregarding interaction with other amino acid residues. (For interpretation of the references to colour in this figure legend, the reader is referred to the web version of this article.)

insights into the impact on the local protein dynamics on the rotamers populated at each site. Such information is completely lost when analyzing a single X-ray model (see stars in Fig. 2D).

Wild type crystallin has 6 natural cysteines (Table 2) and in this study, a surface-accessible cysteine was additionally introduced at position 73, either in the variant S73C (7 total cysteines) or in the variant C111S-S73C (6 total cysteines). Table 2 shows that in the X-ray structure (numbers in italics), only C111 and S73C have a high number of populated rotamers when labelled with MAP or BASL, suggesting high labelling efficiency at those sites. All other cysteines have only one populated rotamer, suggesting a low probability of labelling. If MTSL is used, the two cysteines 73 and 111 remain the most accessible, but other positions (C33, C109, C19) show 2, 4 and 9 rotamers populated, respectively. We previously showed [64] that, when using a 1:1 stoichiometric ratio of MAP vs protein, we could specifically label either the natural C111 in the wild type crystallin, or the S73C in the variant C111S-S73C, corroborating the suggested labelling probabilities based on the rotamer analysis of the crystal structure. However, when considering the 80 snapshots of the MD trajectory, it became apparent that the average number of MAP and BASL rotamers increased for C19 and C109, indicating that in some conformations, the protein can accommodate more than one rotamer (Table 2). The same increase was observed for the MTSL rotamers at those two positions. This finding might suggest that those two positions can become accessible when using a higher stoichiometric ratio of label-to-protein due to the intrinsic dynamics of the backbone and sidechains in the vicinity.

3.2. *Labelling efficiencies and rotational dynamics*

While the *in silico* rotamer analysis might provide hints about the potential accessibility of different labelling sites (Table 2), the actual accessibility of each label towards a cysteine needs to be tested experimentally. In fact, as shown in Fig. 2, structures from the same ensemble might arise from only a few to more than 100 rotamers populated at one specific site. Therefore, an accurate *in silico* prediction of the labelling efficiency is generally not feasible, especially if only one structural model is available.

The protein Bid showed <25 rotamers attached to the two natural cysteines (Fig. 2B), however, the actual labelling efficiency for both MTSL and MAP was high (close to 200 % label per protein for MAP and 160 % for MTSL, see Fig. 3). Labelling with BASL at (pH 8.3) had the lowest efficiency (95 % label per protein, see Fig. 3). A possible explanation for the discrepancy between low rotamer numbers and high labelling efficiency (for MAP and MTSL) could be the poor sampling of the position of the dynamic loops of the protein close to the labelling sites.

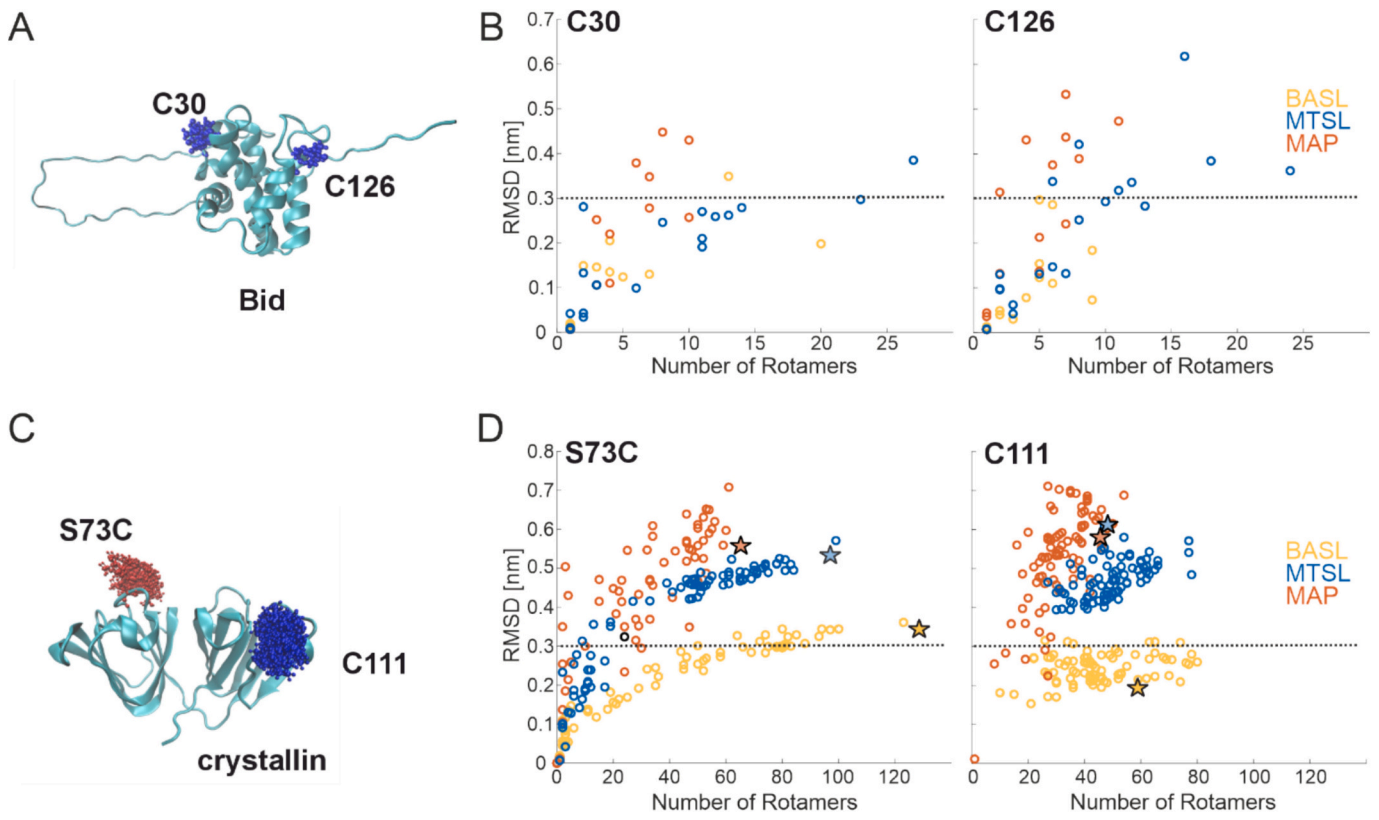

Fig. 2. MMM rotamer analysis of BASL vs MAP and MTSL labels attached to Bid and crystallin. A) NMR structure of Bid (PDB:1DDB, model #1) with BASL rotamers (ball and stick) attached to natural cysteines 30 and 126 (blue). B) Analysis of the spread (rmsd of the nitroxide spin) of BASL (yellow), MAP (red) and MTSL (teal) attached to C30 and C126 on the 20 NMR models of Bid versus the number of rotamers populated. Only models with at least one rotamer populated at each position are shown. A dotted line at 0.3 nm rmsd is drawn to guide the eye. C) X-ray structure of crystallin (PDB:1HK0) with BASL rotamers attached to the exposed natural cysteine C111 (blue) and the engineered cysteine S73C (red). The rotamer analysis with the three labels attached to all natural cysteines and to the S73C is presented in Table 2. D) Rmsd analysis of the spread of the nitroxide spin (rmsd) of BASL (yellow), MAP (red) and MTSL (teal) versus the number of populated rotamers performed on 80 structures extracted from snapshots of a MD trajectory of crystallin in explicit water. As comparison, the data from the crystal structure (PDB:1HK0) are shown as stars. A dotted line at 0.3 nm rmsd is drawn to guide the eye. (For interpretation of the references to colour in this figure legend, the reader is referred to the web version of this article.)

Table 2
Average number of rotamers for the natural cysteines (positions 19, 33, 42, 79, 109, 111, according to UniProt ID: P07320 · CRGD_HUMAN) and for the serine 73 engineered to cysteine (numbering according to UniProt) calculated with the 298 K rotamer library of MMM for the three labels. The presented number of rotamers is an average over the 80 randomly chosen snapshots of the MD trajectory of crystallin. In italics, the number of rotamers calculated on the available crystal structure (PDB:1HK0). In grey, the cysteines with the highest number of populated rotamers, presented in Fig. 2, are highlighted. Note that in the PDB: 1HK0 the cysteines 19, 33, 42, 79 are wrongly numbered as 18, 32, 41, 78 and the serine 73 is wrongly numbered as 72.

	C19	C33	C42	C79	C109	C111	S73C
BASL ensemble	1.6	0.7	0.7	1.0	1.6	45.3	36.8
X-ray structure	*1*	*1*	*1*	*1*	*1*	*59*	*129*
MAP ensemble	1.6	0.1	0.4	0.2	2.0	31.1	24.9
X-ray structure	*1*	*1*	*1*	*1*	*1*	*45*	*64*
MTSL ensemble	9.5	0.5	0.8	0.9	9.1	49.4	41.6
X-ray structure	*9*	*2*	*1*	*1*	*4*	*48*	*96*

For crystallin, the variant S73C (containing 7 cysteines) was spin labelled with a 2:1 label-to-protein ratio to specifically target only the two most accessible cysteines (C111 and S73C). Despite the low stoichiometric ratio used, the labelling was successful with both BASL and MAP at the same pH 7.5 (120 and 130 % label per protein). This indicates that labelling with BASL is feasible also at physiological pH (Fig. S2). Intriguingly, the labelling with MTSL did not work on two biological repeats. We surmise that the presence of adjacent natural cysteines might have interfered with the MTSL binding, inducing intra-protein cross-linking.

3.3. *Interspin distances*

We performed DEER on the spin-labelled proteins to compare the interspin distance distributions for all three labels (for crystallin, the MTSL-labelled sample was omitted due to the poor labelling efficiency). Bid labelled with MTSL showed a high modulation depth of the dipolar signal (35 %, Fig. 4A), corresponding to the high labelling efficiency detected (160 % per protein, in average 80 % per cysteine, Fig. 3B), and a bimodal interspin distance distribution, which was previously detected on other biological repeats [11,65,66]. Bid labelled with MAP (modulation depth 30 %) and BASL (modulation depth 12 %) showed a narrow monomodal distribution, with modulation depths in line with the respective labelling efficiency (Figs. 3B and 4A). Comparison of the three distance distributions proves that the bimodality observed with MTSL arises from label's and not from protein's rearrangements. This is one of the advantages of comparing different labels on the same sites [58]. The simulated distances on the 20 NMR models agree well with the experimental distance of MAP and BASL but cannot predict the main peak detected experimentally with MTSL, indicating that the preferred orientations of the MTSL sidechain in the frozen structure are not captured by the 298 K rotamer library in any model of the NMR ensemble.

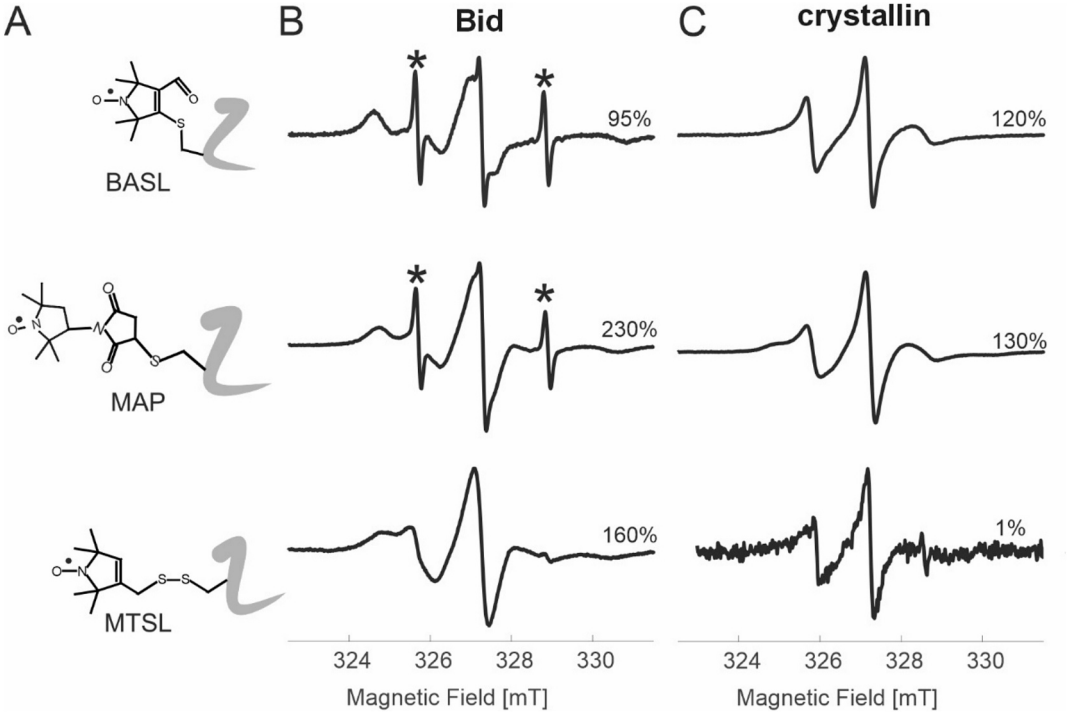

Fig. 3. X-band cw EPR spectra of different spin-labelled variants. A) Structure of the three different nitroxide labels attached to a protein backbone. B) Room temperature X-band cw EPR spectra for Bid wild type (two natural cysteines C30 and C126). Spin labelling efficiencies (uncertainties ±10 %, considering the errors in the double integration and the small variability observed in two repeats) are given as spin per protein concentration (for Bid, the maximum expected value is 200 %). Stars denote the low and high field peaks of residual free label in two Bid samples, which causes a slight overestimation of the labelling efficiency. C) Room temperature X-band cw EPR spectra for the S73C crystallin variant (containing 7 cysteines) labelled at 2:1 label-to-protein ratio (targeting the two most accessible cysteines C111 and S73C, see Table 2). The labelling with MTSL failed on two biological repeats. Spin labelling efficiencies (uncertainties ±10 %, considering the errors in the double integration and the variability observed in two repeats) are given as spin per protein concentration (the maximum theoretical labelling efficiency for crystallin is given by the label-to-protein stoichiometric ratio used, which is 220 %, due to the 2.2:1 stoichiometric ratio used).

The wild type γD-crystallin contains six natural cysteines, but it was previously shown that at 2:1 label-to-protein stoichiometric ratio, the dipolar modulation observed on the S73C variant (with six natural cys and one engineered cys) is due to the selective labelling of the natural C111 and the engineered S73C [64]. The obtained modulation depth (30 %) is too high for a labelling efficiency of only 130 % with MAP, implying that other cysteines might have been labelled as well (Figs. 3C and 4B). The distance distribution was found to be broad, with a full width at half maximum of about 1.5 nm (Fig. 4B). The distance distribution did no change when PEG6000 was used as cryoprotectant, while a bimodal distribution appeared when using 30 % *v/v* glycerol in the solution [64]. Intriguingly, the modulation depth of BASL-labelled crystallin (9 %) was only one third of that observed for MAP-labelled protein (30 %), despite the two samples having very similar total labelling efficiencies (Figs. 3C and 4B). This finding suggested preferential labelling of one of the two most accessible positions by BASL, which will be discussed later.

The simulated distance distributions obtained on 20 snapshots of the MD trajectory with MMM [46] and on the entire MD trajectory with DEERPREdict [62] lie within the experimentally observed width of the distance distribution for MAP, with the width of the simulated distance distribution being a bit larger when the whole MD trajectory is considered. In contrast to MAP-labelled crystallin, the BASL-labelled protein is characterized by a narrow monomodal distance distribution with a full width at half maximum of about 0.7 nm (Fig. 4B), in good agreement with the rotamer simulations on the ensemble. Notably, for BASL, the DEERPREdict simulation performed on the entire trajectory is almost indistinguishable from the MMM simulation obtained on 20 snapshots [46], which suggests optimal sampling of the conformations of BASL in the rotamer library. When simulating the distance distributions on a single structure of crystallin (Fig. S3) with MMM or DEERPREdict, we observed some discrepancies for MAP, probably due to the use of different force fields to calculate the Lennard-Jones potential in the two softwares [46,62] while for MTSL and BASL the distance distributions were minimally affected highlighting a more robust output for those two labels with different softwares.

3.4. *Site- and surface-selectivity of BASL vs MAP on γD-crystallin*

Based on the low modulation depth observed in the DEER traces of the BASL-labelled S73C variant (Fig. 4B), we decided to further address the possible selectivity of BASL with respect to the two most accessible positions in crystallin by separately analyzing variants containing only one of the two most accessible cysteine residues at a time. The variants C111S-S73C (containing only the accessible S73C) and the wild type (containing only the accessible C111) were labelled with both MAP and BASL using a 1:1 label-to-protein ratio. The X-band cw EPR spectra (Fig. 5) highlight the distinct dynamics of the two labels attached to each site. The MAP label at position 73 has a spectrum with two components (red), while BASL shows a more ‘mobile’ spectral shape, characterized by one main spectral component (black). In contrast, it is the MAP label at position 111 to have a more ‘mobile’ spectral shape than BASL. This highlights the label-dependent dynamics and further strengthens the idea that having more labels at disposal can contribute to a better understanding of the dynamics at different sites. Interestingly, the labelling efficiency of the C111S-S73C variant is similarly high with both MAP and BASL 85 and 80 %, respectively. In contrast, the wild type crystallin (with the accessible C111) has a high labelling efficiency with MAP (85 %) but a very poor labelling efficiency with BASL (10 %). Therefore, under the same experimental conditions, MAP can label efficiently both sites (85 %) but BASL can efficiently label S73C (80 %) but only poorly C111 (10 %). The labelling efficiencies clearly point to a site-specificity

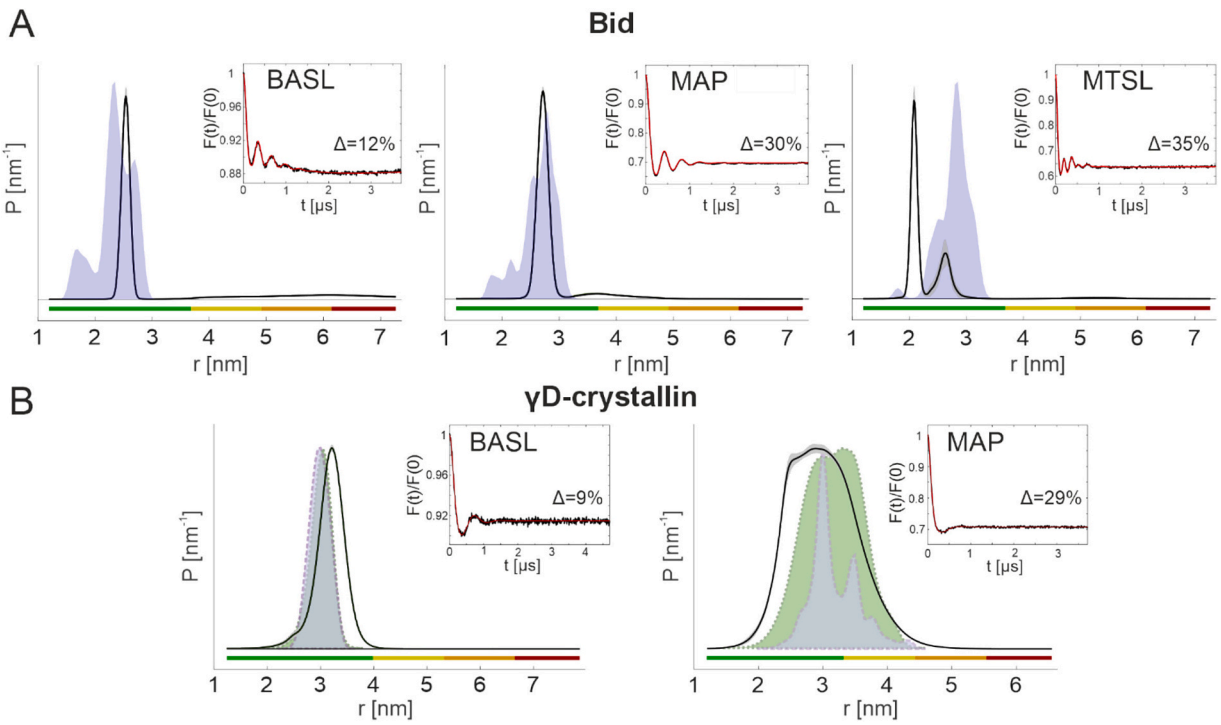

Fig. 4. Distance distributions from different labels. A) Deer analysis on double cysteine variant of Bid with three different spin labels. Experimental distance distributions (black lines, with grey shades representing the uncertainty) compared with the distance distribution simulated (blue areas) with MMM on the ensemble of 20 structures (PDB: 1DDB). B) Deer analysis on the S73C variant of γD-crystallin. The experimental distance distributions (black lines) are compared with the distance distributions simulated with MMM (blue areas) and simulated with DEERPREdict (green) using only the two surface exposed cysteines C111 and S73C on 20 snapshots randomly chosen on the MD trajectory. Insets show the DEER form factor with the fit obtained with DEERNet and the corresponding modulation depths (Δ). Primary data are shown in Fig. S4. (For interpretation of the references to colour in this figure legend, the reader is referred to the web version of this article.)

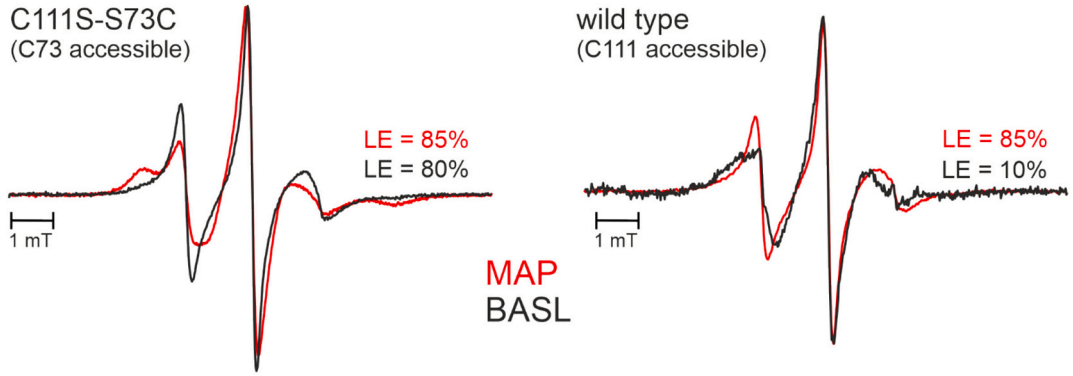

Fig. 5. Site-selective labelling of BASL on crystallin. Amplitude-normalized X-band cw EPR spectra of the C111S-C73 variant, left, carrying the accessible C73 and of the wild type, right, carrying the accessible C111. Labelling conditions: 1:1 label-to-protein ratio for BASL (black) and MAP (red) as described in Materials and Methods. (For interpretation of the references to colour in this figure legend, the reader is referred to the web version of this article.)

of BASL towards the cysteine at position 73.

To further verify that BASL has a labelling preference for C73 (site-specificity) and yet it maintains its surface-selectivity ability, we labelled the C111S-S73C variant (7 total cysteines) at increasing label-to-protein ratios and performed DEER experiments (Fig. 6). At a 1:1 protein-to-label ratio (Fig. 6A), no dipolar oscillations could be detected, confirming that S73C is the only accessible cysteine for MAP and BASL at the chosen experimental conditions. However, when the label-to-protein stoichiometric ratio was increased to 2:1 and 4:1, we observed increasing dipolar modulations for the MAP-labelled samples, indicating that MAP at higher stoichiometric ratios can label the S73C as well as other cysteines which are less surface exposed. In stark contrast, increasing the stoichiometric ratio of BASL did not cause the appearance of dipolar modulations, confirming the exquisite specificity of BASL for surface accessible cysteines (Fig. 6A). The distance distribution obtained from the 2:1 and 4:1 MAP-labelled samples showed two main peaks at 3.2 and 3.8 nm (Fig. 6B), with the intensity of the short distance peak increasing relatively to the long peak at higher labelling ratios. Fig. 6C highlights the possible natural cysteine candidates for MAP labelling at high stoichiometric ratio, based on the rotamer analysis shown in Table 2. The crystallin variant under study has no C111, therefore, the observed distances are due to pairs between C73 (most accessible) and another natural cysteine. Additional analysis of the wild type crystallin and of the S73C variant (Fig. S5) confirmed that C109 is labelled (due to the fingerprint short distance to C111 in the wild type sample and in the S73C variant), while assignment of the additional labelled natural cysteines is not straightforward, due to overlap between the corresponding distance distributions (Fig. S5D).

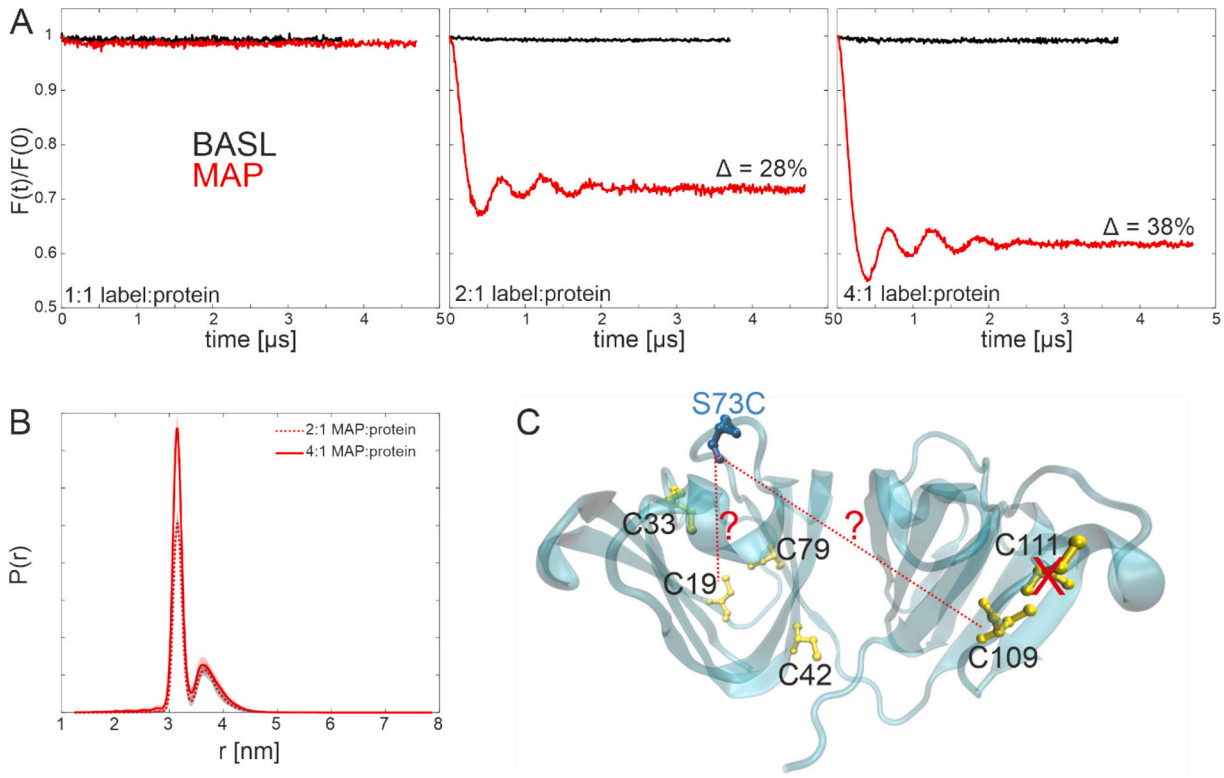

Fig. 6. Surface specificity of BASL. A) DEER form factors for the C111S-S73C crystallin variant labelled with BASL (black) and MAP (red) at different label-to-protein ratios. Left: at 1:1 label-to-protein ratio the absence of dipolar modulation confirms that the only labelled cysteine is S73C (85 % and 80 % labelling efficiency expressed as label per protein for MAP and BASL, respectively, see Fig. 5). Middle: with 2-fold label-to-protein ratio (labelling efficiency 162 % and 74 % for MAP and BASL, respectively) the appearance of dipolar oscillations and a modulation depth of 28 % confirms that MAP, but not BASL can label additional natural cysteines. Right: with 4-fold label-to-protein ratio (labelling efficiency 229 % and 84 % for MAP and BASL, respectively) the modulation depth further increases for MAP, indicating further labelling of the natural cysteines. B) Distance distributions of the MAP-labelled variant with 2:1 (red dotted line, in shaded grey the uncertainty) and 4:1 (red line, in shaded red the uncertainty). C) Representation of crystallin with 7 cysteines. The engineered C73 is highlighted in blue, C111 is not present in the variant studied (crossed out). The possible distances between C73 and the two natural cysteines with >1 rotamer in Table 2 are highlighted. Primary data and distance analysis on other crystallin variants are shown in Fig. S5. (For interpretation of the references to colour in this figure legend, the reader is referred to the web version of this article.)

3.5. *Site-selectivity for orthogonal labelling*

The exceptional surface specificity of BASL, and its preferential labelling towards C73 with respect to C111 prompted us to explore an orthogonal labelling approach on the S73C variant combining two cys-targeting labels: a nitroxide spin label (BASL) and a maleimide Gd (III)-DOTA spin label. For comparison, the same protocol was repeated with the non-surface-specific, non-site-specific MAP.

Exploiting the high specificity of BASL for S73C, the label was first added in a 1:1 ratio to the S73C variant. After washing out the residual BASL label, maleimide Gd-DOTA was added in a 1:1 ratio. The same procedure was repeated using MAP and subsequently the maleimide Gd-DOTA label. Both samples were then analyzed using the three-DEER-channel methodology previously described in detail for orthogonally labelled samples [22]. The corresponding nitroxide-nitroxide (NO-NO), gadolinium-gadolinium (Gd—Gd) and gadolinium-nitroxide (Gd-NO) DEER traces are shown in Fig. 7 (with primary data in Figs. S7). The modulation depth of each sample is compared to the maximal modulation depth in each channel obtained under the same experimental conditions (horizontal dotted line in each panel of Fig. 7, obtained from the primary DEER data shown in Fig. S6) on the biradicals previously used for the analysis of the three-channel DEER performance and the identification of possible artefacts [22]. Based on the detected BASL specificity towards C73, the BASL-labelled sample was expected to exhibit a modulation depth in the NO-NO and Gd—Gd samples lower than that of the MAP-labelled analogue and a modulation depth of the Gd-NO DEER traces higher than the MAP-analogue.

The specificity of BASL towards C73 could be confirmed by a modulation depth of only 4 % in the NO-NO DEER trace, lower than that obtained with the MAP labelling (11 %). In both cases the distance distribution is comparable to that obtained with the usual labelling procedure (see Fig. 4B). The same trend is also visible for the Gd—Gd distances, with the BASL labelling method displaying a modulation depth of 1.2 %, lower than that detected with MAP (1.8 %). The mean Gd—Gd distance of 3.2 nm is in line with the simulated Gd—Gd distances. The additional peak below 2 nm, which was also observed for the 5-nm Gd—Gd ruler (Fig. S6), is due to the presence of a minor ($\Delta \sim 0.5$ %) artefact present in the setup used, which becomes more visible relative when distances with low modulation depths are analyzed, as in this case. Finally, the NO-Gd DEER shows the expected inverted trend, with a modulation depth of 4 % for the MAP- labelled variant and of 14 % for the BASL-labelled analogue. The distance distribution is in good agreement with the simulated BASL-Gd distance. Therefore, despite not being perfectly selective, the high site-specificity of BASL towards one specific cysteine at the surface of a protein enabled detection of intra-protein orthogonal distance with higher sensitivity than that obtainable by a statistical distribution of the two orthogonal spin labels in the two cysteine sites.

4. Conclusions

Having a broad range of spin labels at hand with different chemical properties is crucial to best access properties of biomolecules, such as dynamics or distance distributions. Here we presented an *in silico* and *in*

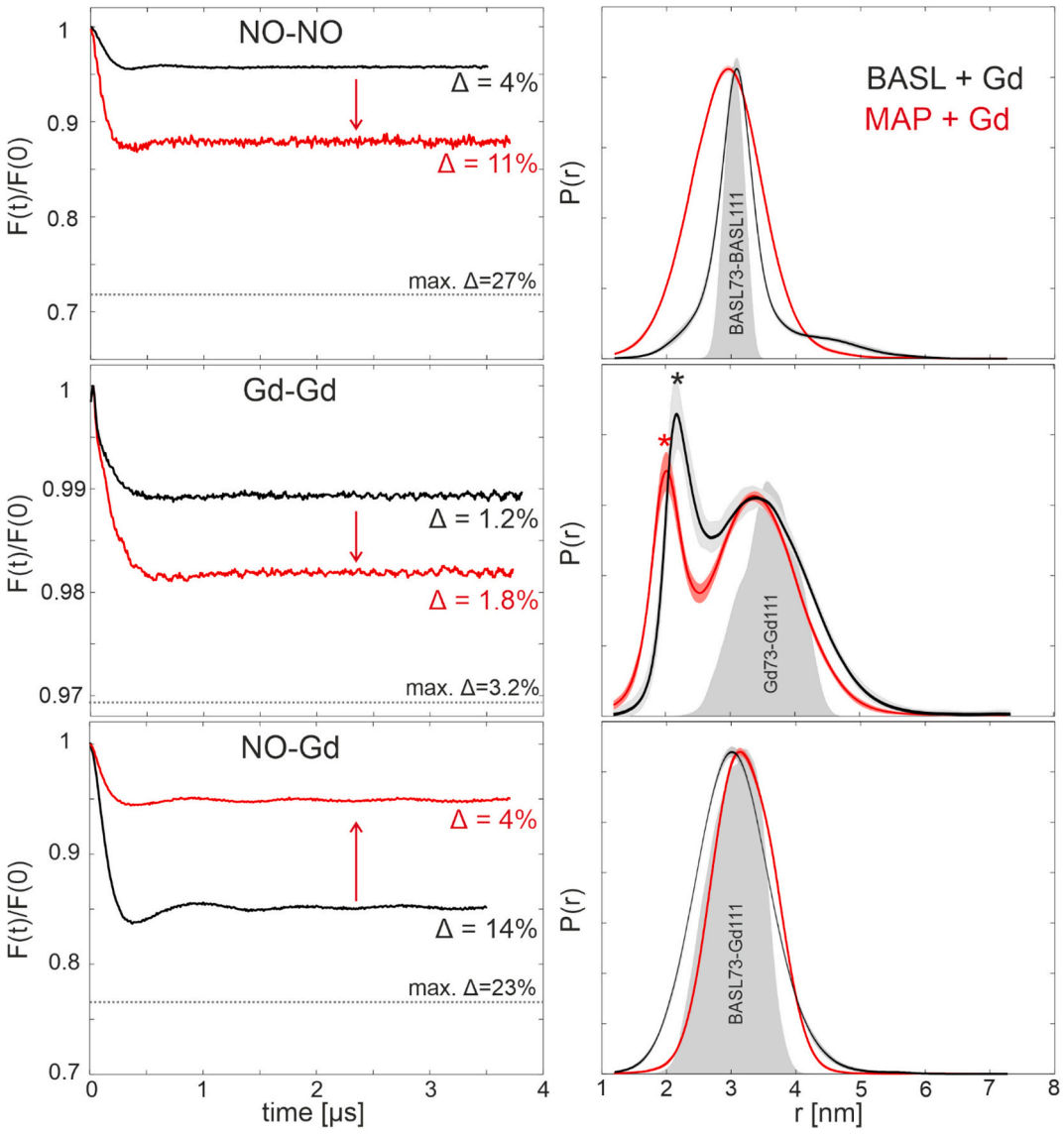

Fig. 7. BASL specificity allows preferential orthogonal labelling of crystallin at positions 111 and 73. The double cysteine variant was labelled with either BASL and maleimide-Gd(DOTA) in a 1:1 ratio (black) or with MAP and maleimide-Gd(DOTA in a 1:1 ratio (red). Details of the labelling procedure are described in the Materials and Methods. A) Form factors and modulation depths obtained from DEER traces using the setup to selectively measure nitroxide-nitroxide distances (NO-NO setup). The maximum expected modulation depth detected using the same setup on a nitroxide-nitroxide ruler is shown as horizontal dotted line. The distance distributions with uncertainties (shaded areas) are obtained via DEERNet and are shown on the right. B) DEER analysis on the same sample using the Gd—Gd setup. The maximum modulation depth was obtained under the same experimental conditions on a Gd—Gd ruler. The asterisk in the distance distributions on the right indicates a short distance peak possibly arising from partial aggregation in the sample. C) DEER analysis on the same sample using the NO-Gd setup. The maximum modulation depth was obtained under the same experimental conditions on a Gd-NO ruler. Distance distributions are shown on the right. A simulation of the S73C-BASL and C111—Gd distance is shown in grey. Due to the specificity of BASL, the modulation depth of the homo-distances (NO-NO and Gd—Gd) decreases with respect to MAP, while the modulation depth of the hetero-distances increases with respect to the sample labelled with MAP. The DEER analysis of the Gd-rulers is presented in Fig. S6, the primary DEER traces of the crystallin samples are shown in Fig. S7. (For interpretation of the references to colour in this figure legend, the reader is referred to the web version of this article.)

vitro characterization of three nitroxide-based spin labels (BASL, MTSL and MAP) attached to Bid and crystallin, showcasing the characteristic features of BASL, such as rigidity, surface accessibility and site specificity.

We demonstrated that the labelling efficiency for BASL varies depending on the chosen site, but the reaction can be effective also at physiological pH. The novel rotamer library of BASL captures well the increased rigidity of BASL with respect to MAP and MTSL. The distance distributions obtained with BASL were monomodal and with a narrow characteristic distribution width, which can be pivotal for assessing minor conformational changes in proteins, or creating coarse-grained models based on precise distance constraints. Additionally, disordered regions of proteins characterized by large widths of the distance distributions might be more accurately described using BASL than the more flexible MTSL or MAP.

Having at disposal ensemble structures (NMR or MD simulations) is beneficial for a more comprehensive analysis of the labelling probabilities of the chosen sites, and we demonstrated the key feature of BASL to selectively label only exposed cysteines in the presence of several natural cysteines in a protein even at higher label excess. Beyond the surface selectivity, we found that BASL has an unforeseen site specificity, which can be exploited for an increase sensitivity in detecting intra-protein distances via site-directed orthogonal spin labelling.

CRediT authorship contribution statement

Dominik Gendreizig: Writing – review & editing, Writing – original draft, Visualization, Investigation, Formal analysis, Data curation. **Christina Elsner:** Writing – original draft, Visualization, Formal analysis, Data curation. **Svetlana Kucher:** Writing – review & editing, Writing – original draft, Visualization, Validation, Supervision, Formal analysis, Data curation. **Gunnar Jeschke:** Writing – review & editing, Software. **Alistair J. Fielding:** Writing – review & editing, Writing – original draft, Conceptualization. **Enrica Bordignon:** Writing – review & editing, Writing – original draft, Validation, Supervision, Resources, Project administration, Funding acquisition, Data curation, Conceptualization.

Declaration of competing interest

The authors declare that they have no known competing financial interests or personal relationships that could have appeared to influence the work reported in this paper.

Acknowledgement

E.B. and D.G. thanks Lars V Schäfer, Saumyak Mukherjee and Simon L Holtbrügge for providing the snapshots from the MD trajectories of crystallin. E.B. and S.K. thank Giulio Tesei for implementing MMMx libraries for MTSL, MAP and BASL in DEERPREdict. A.J.F. thanks Michael A. Hollas for the sample of BASL. This work is supported by the SNSF grant number 188817.

Appendix A. Supplementary data

Supplementary data to this article can be found online at https://doi.org/10.1016/j.jmr.2025.107953.

Data availability

Data will be made available on request.

References

[1] W.L. Hubbell, C.J. Lopez, C. Altenbach, Z. Yang, Technological advances in site-directed spin labeling of proteins, Curr. Opin. Struct. Biol. 23 (5) (2013) 725–733, https://doi.org/10.1016/j.sbi.2013.06.008.
[2] G. Jeschke, DEER distance measurements on proteins, Annu. Rev. Phys. Chem. 63 (2012) 419–446, https://doi.org/10.1146/annurev-physchem-032511-143716.
[3] L. Galazzo, E. Bordignon, Electron paramagnetic resonance spectroscopy in structural-dynamic studies of large protein complexes, Prog. Nucl. Magn. Reson. Spectrosc. 134-135 (2023) 1–19, https://doi.org/10.1016/j.pnmrs.2022.11.001.
[4] A. Bonucci, O. Ouari, B. Guigliarelli, V. Belle, E. Mileo, In-cell EPR: Progress towards structural studies inside cells, Chembiochem 21 (4) (2020) 451–460, https://doi.org/10.1002/cbic.201900291.
[5] A.J. Fielding, M.G. Concilio, G. Heaven, M.A. Hollas, New developments in spin labels for pulsed dipolar EPR, Molecules 19 (10) (2014) 16998–17025, https://doi.org/10.3390/molecules191016998.
[6] L. Galazzo, M. Teucher, E. Bordignon, Orthogonal spin labeling and pulsed dipolar spectroscopy for protein studies, Methods Enzymol. 666 (2022) 79–119, https://doi.org/10.1016/bs.mie.2022.02.004.
[7] F. Torricella, A. Pierro, E. Mileo, V. Belle, A. Bonucci, Nitroxide spin labels and EPR spectroscopy: a powerful association for protein dynamics studies, Biochim. Biophys. Acta, Proteins Proteomics 1869 (7) (2021) 140653, https://doi.org/10.1016/j.bbapap.2021.140653.
[8] E. Bordignon, EPR spectroscopy of Nitroxide spin probes, In *eMagRes* (2017) 235–254.
[9] W.L. Hubbell, C. Altenbach, Investigation of structure and dynamics in membrane-proteins using site-directed spin-labeling, Curr. Opin. Struct. Biol. 4 (4) (1994) 566–573, https://doi.org/10.1016/S0959-440x(94)90219-4.
[10] L.J. Berliner, J. Grunwald, H.O. Hankovszky, K. Hideg, A novel reversible thiol-specific spin label: papain active site labeling and inhibition, Anal. Biochem. 119 (2) (1982) 450–455, https://doi.org/10.1016/0003-2697(82)90612-1.
[11] S. Bleicken, T.E. Assafa, H. Zhang, C. Elsner, I. Ritsch, M. Pink, S. Rajca, G. Jeschke, A. Rajca, E. Bordignon, Gem-diethyl pyrroline nitroxide spin labels: synthesis, EPR characterization, rotamer libraries and biocompatibility, ChemistryOpen 8 (8) (2019) 1057–1065, https://doi.org/10.1002/open.201900119.
[12] J.T. Paletta, M. Pink, B. Foley, S. Rajca, A. Rajca, Synthesis and reduction kinetics of sterically shielded pyrrolidine nitroxides, Org. Lett. 14 (20) (2012) 5322–5325, https://doi.org/10.1021/ol302506f.
[13] G. Karthikeyan, A. Bonucci, G. Casano, G. Gerbaud, S. Abel, V. Thomé, L. Kodjabachian, A. Magalon, B. Guigliarelli, V. Belle, et al., A bioresistant nitroxide spin label for in-cell EPR spectroscopy: in vitro and in oocytes protein structural dynamics studies, Angew. Chem. Int. Ed. 57 (5) (2018) 1366–1370, https://doi.org/10.1002/anie.201710184.
[14] N. Fleck, C. Heubach, T. Hett, S. Spicher, S. Grimme, O. Schiemann, Ox-SLIM: synthesis of and site-specific labelling with a highly hydrophilic Trityl spin label, Chemistry 27 (16) (2021) 5292–5297, https://doi.org/10.1002/chem.202100013.
[15] S. Ketter, A. Gopinath, O. Rogozhnikova, D. Trukhin, V.M. Tormyshev, E. G. Bagryanskaya, B. Joseph, In situ labeling and distance measurements of membrane proteins in E. Coli using Finland and OX063 Trityl labels, Chemistry 27 (7) (2021) 2299–2304, https://doi.org/10.1002/chem.202004606.
[16] A. Martorana, G. Bellapadrona, A. Feintuch, E. Di Gregorio, S. Aime, D. Goldfarb, Probing protein conformation in cells by EPR distance measurements using Gd3+ spin labeling, J. Am. Chem. Soc. 136 (38) (2014) 13458–13465, https://doi.org/10.1021/ja5079392.
[17] D. Goldfarb, Gd3+ spin labeling for distance measurements by pulse EPR spectroscopy, Phys. Chem. Chem. Phys. 16 (21) (2014) 9685–9699, https://doi.org/10.1039/c3cp53822b.
[18] M. Ji, S. Ruthstein, S. Saxena, Paramagnetic metal ions in pulsed ESR distance distribution measurements, Acc. Chem. Res. 47 (2) (2014) 688–695, https://doi.org/10.1021/ar400245z.
[19] J.L. Wort, K. Ackermann, A. Giannoulis, A.J. Stewart, D.G. Norman, B.E. Bode, Sub-micromolar pulse dipolar EPR spectroscopy reveals increasing cu(II) -labelling of double-histidine motifs with lower temperature, Angew. Chem. Int. Ed. 58 (34) (2019) 11681–11685, https://doi.org/10.1002/anie.201904848.
[20] T.F. Cunningham, M.R. Putterman, A. Desai, W.S. Horne, S. Saxena, The double-histidine cu(2)(+)-binding motif: a highly rigid, site-specific spin probe for electron spin resonance distance measurements, Angew. Chem. Int. Ed. Eng. 54 (21) (2015) 6330–6334, https://doi.org/10.1002/anie.201501968.
[21] L. Garbuio, E. Bordignon, E.K. Brooks, W.L. Hubbell, G. Jeschke, M. Yulikov, Orthogonal spin labeling and Gd(III)-nitroxide distance measurements on bacteriophage T4-lysozyme, J. Phys. Chem. B 117 (11) (2013) 3145–3153, https://doi.org/10.1021/jp401806g.
[22] M. Teucher, M. Qi, N. Cati, H. Hintz, A. Godt, E. Bordignon, Strategies to identify and suppress crosstalk signals in double electron-electron resonance (DEER) experiments with gadolinium(III) and nitroxide spin-labeled compounds, Magn Reson 1 (2) (2020) 285–299, https://doi.org/10.5194/mr-1-285-2020.
[23] I. Kaminker, H. Yagi, T. Huber, A. Feintuch, G. Otting, D. Goldfarb, Spectroscopic selection of distance measurements in a protein dimer with mixed nitroxide and Gd3+ spin labels, Phys. Chem. Chem. Phys. 14 (13) (2012) 4355–4358, https://doi.org/10.1039/c2cp40219j.
[24] Y. Polyhach, E. Bordignon, G. Jeschke, Rotamer libraries of spin labelled cysteines for protein studies, Phys. Chem. Chem. Phys. 13 (6) (2011) 2356–2366, https://doi.org/10.1039/c0cp01865a.
[25] G. Hagelueken, R. Ward, J.H. Naismith, O. Schiemann, Mtsslwizard: in silico spin-labeling and generation of distance distributions in PyMOL, Appl. Magn. Reson. 42 (3) (2012) 377–391, https://doi.org/10.1007/s00723-012-0314-0.
[26] J.L. Sarver, J.E. Townsend, G. Rajapakse, L. Jen-Jacobson, S. Saxena, Simulating the dynamics and orientations of spin-labeled side chains in a protein-DNA complex, J. Phys. Chem. B 116 (13) (2012) 4024–4033, https://doi.org/10.1021/jp211094n.
[27] F. Tombolato, A. Ferrarini, J.H. Freed, Dynamics of the nitroxide side chain in spin-labeled proteins, J. Phys. Chem. B 110 (51) (2006) 26248–26259, https://doi.org/10.1021/jp0629487.
[28] F. Tombolato, A. Ferrarini, J.H. Freed, Modeling the effects of structure and dynamics of the nitroxide side chain on the ESR spectra of spin-labeled proteins, J. Phys. Chem. B 110 (51) (2006) 26260–26271, https://doi.org/10.1021/jp062949z.
[29] D. Sezer, J.H. Freed, B. Roux, Parametrization, molecular dynamics simulation, and calculation of electron spin resonance spectra of a nitroxide spin label on a polyalanine alpha-helix, J. Phys. Chem. B 112 (18) (2008) 5755–5767, https://doi.org/10.1021/jp711375x.
[30] H.S. McHaourab, M.A. Lietzow, K. Hideg, W.L. Hubbell, Motion of spin-labeled side chains in T4 lysozyme. Correlation with protein structure and dynamics, Biochemistry 35 (24) (1996) 7692–7704, https://doi.org/10.1021/bi960482k.
[31] H. Steinhoff, A. Savitsky, C. Wegener, M. Pfeiffer, M. Plato, K. Mobius, High-field EPR studies of the structure and conformational changes of site-directed spin labeled bacteriorhodopsin, Biochim. Biophys. Acta 1457 (3) (2000) 253–262, https://doi.org/10.1016/s0005-2728(00)00106-7.
[32] N.L. Fawzi, M.R. Fleissner, N.J. Anthis, T. Kalai, K. Hideg, W.L. Hubbell, G. M. Clore, A rigid disulfide-linked nitroxide side chain simplifies the quantitative analysis of PRE data, J. Biomol. NMR 51 (1–2) (2011) 105–114, https://doi.org/10.1007/s10858-011-9545-x.
[33] M.R. Fleissner, M.D. Bridges, E.K. Brooks, D. Cascio, T. Kalai, K. Hideg, W. L. Hubbell, Structure and dynamics of a conformationally constrained nitroxide side chain and applications in EPR spectroscopy, Proc. Natl. Acad. Sci. USA 108 (39) (2011) 16241–16246, https://doi.org/10.1073/pnas.1111420108.
[34] O.H. Griffith, H.M. McConnell, A nitroxide-maleimide spin label, Proc. Natl. Acad. Sci. USA 55 (1) (1966) 8–11, https://doi.org/10.1073/pnas.55.1.8.
[35] K. Ackermann, A. Chapman, B.E. Bode, A comparison of cysteine-conjugated Nitroxide spin labels for pulse dipolar EPR spectroscopy, Molecules 26 (24) (2021), https://doi.org/10.3390/molecules26247534.

[36] M.R. Fleissner, E.M. Brustad, T. Kalai, C. Altenbach, D. Cascio, F.B. Peters, K. Hideg, S. Peuker, P.G. Schultz, W.L. Hubbell, Site-directed spin labeling of a genetically encoded unnatural amino acid, Proc. Natl. Acad. Sci. USA 106 (51) (2009) 21637–21642, https://doi.org/10.1073/pnas.0912009106.
[37] M.J. Schmidt, A. Fedoseev, D. Bucker, J. Borbas, C. Peter, M. Drescher, D. Summerer, EPR distance measurements in native proteins with genetically encoded spin labels, ACS Chem. Biol. 10 (12) (2015) 2764–2771, https://doi.org/10.1021/acschembio.5b00512.
[38] M.J. Schmidt, A. Fedoseev, D. Summerer, M. Drescher, Genetically encoded spin labels for in vitro and in-cell EPR studies of native proteins, Methods Enzymol. 563 (2015) 483–502, https://doi.org/10.1016/bs.mie.2015.05.023.
[39] G. Heaven, M.A. Hollas, L. Tabernero, A.J. Fielding, Spin labeling of surface cysteines using a Bromoacrylaldehyde spin label, Appl. Magn. Reson. 52 (8) (2021) 959–970, https://doi.org/10.1007/s00723-021-01350-1.
[40] T. Kálai, M. Balog, J. Jekö, K. Hideg, 3-substituted 4-Bromo-2,2,5,5-tetramethyl-2,5-dihydro-1H-pyrrol-1-yloxyl radicals as versatile synthons for synthesis of new paramagnetic heterocycles, Synthesis 1998 (10) (1998) 1476–1482, https://doi.org/10.1055/s-1998-2178.
[41] O. Roopnarine, K. Hideg, D.D. Thomas, Saturation-transfer Electron parametric resonance of an Indane Dione spin-label - calibration with hemoglobin and application to myosin rotational-dynamics, Biophys. J. 64 (6) (1993) 1896–1907, https://doi.org/10.1016/S0006-3495(93)81561-3.
[42] L.I. Horvath, L. Dux, H.O. Hankovszky, K. Hideg, D. Marsh, Saturation transfer Electron-spin-resonance of Ca2+-Atpase covalently spin-labeled with Beta-substituted vinyl ketone-Nitroxide and Maleimide-Nitroxide derivatives - effects of segmental motion and labeling levels, Biophys. J. 58 (1) (1990) 231–241, https://doi.org/10.1016/S0006-3495(90)82368-7.
[43] Esmann M.; Hideg K.; Marsh D., Conventional and saturation transfer Epr spectroscopy of Na+/K+-Atpase modified with different Maleimide-Nitroxide derivatives. Biochim. Biophys. Acta. 1159.151–59. 10.1016/0167-4838(92)90074-n.
[44] E. Kachooei, N.M. Cordina, L.J. Brown, Constructing a structural model of troponin using site-directed spin labeling: EPR and PRE-NMR, Biophys. Rev. 11 (4) (2019) 621–639, https://doi.org/10.1007/s12551-019-00568-5.
[45] M. Chen, T. Kalai, D. Cascio, M.D. Bridges, J.P. Whitelegge, M. Elgeti, W. L. Hubbell, A highly ordered Nitroxide side chain for distance mapping and monitoring slow structural fluctuations in proteins, Appl. Magn. Reson. 55 (1–3) (2024) 251–277, https://doi.org/10.1007/s00723-023-01618-8.
[46] G. Jeschke, MMM: Integrative ensemble modeling and ensemble analysis, Protein Sci. 30 (1) (2021) 125–135, https://doi.org/10.1002/pro.3965.
[47] G. Jeschke, MMM: a toolbox for integrative structure modeling, Protein Sci. 27 (1) (2018) 76–85, https://doi.org/10.1002/pro.3269.
[48] J.M. McDonnell, D. Fushman, C.L. Milliman, S.J. Korsmeyer, D. Cowburn, Solution structure of the proapoptotic molecule BID: a structural basis for apoptotic agonists and antagonists, Cell 96 (5) (1999) 625–634, https://doi.org/10.1016/s0092-8674(00)80573-5.
[49] A. Basak, O. Bateman, C. Slingsby, A. Pande, N. Asherie, O. Ogun, G.B. Benedek, J. Pande, High-resolution X-ray crystal structures of human gammaD crystallin (1.25 a) and the R58H mutant (1.15 a) associated with aculeiform cataract, J. Mol. Biol. 328 (5) (2003) 1137–1147, https://doi.org/10.1016/s0022-2836(03)00375-9.
[50] S. Desagher, A. Osen-Sand, A. Nichols, R. Eskes, S. Montessuit, S. Lauper, K. Maundrell, B. Antonsson, J.C. Martinou, Bid-induced conformational change of Bax is responsible for mitochondrial cytochrome c release during apoptosis, J. Cell Biol. 144 (5) (1999) 891–901, https://doi.org/10.1083/jcb.144.5.891.
[51] S. Mukherjee, S. Ramos, S. Pezzotti, A. Kalarikkal, T.M. Prass, L. Galazzo, D. Gendreizig, N. Barbosa, E. Bordignon, M. Havenith, et al., Entropy tug-of-war determines solvent effects in the liquid-liquid phase separation of a globular protein, J. Phys. Chem. Lett. 15 (15) (2024) 4047–4055, https://doi.org/10.1021/acs.jpclett.3c03421.
[52] R. Tschaggelar, B. Kasumaj, M.G. Santangelo, J. Forrer, P. Leger, H. Dube, F. Diederich, J. Harmer, R. Schuhmann, I. Garcia-Rubio, et al., Cryogenic 35GHz pulse ENDOR probehead accommodating large sample sizes: performance and applications, J. Magn. Reson. 200 (1) (2009) 81–87, https://doi.org/10.1016/j.jmr.2009.06.007.
[53] M. Teucher, E. Bordignon, Improved signal fidelity in 4-pulse DEER with Gaussian pulses, J. Magn. Reson. 296 (2018) 103–111, https://doi.org/10.1016/j.jmr.2018.09.003.
[54] C.E. Tait, S. Stoll, Coherent pump pulses in double Electron Electron resonance spectroscopy, Phys. Chem. Chem. Phys. 18 (27) (2016) 18470–18485, https://doi.org/10.1039/c6cp03555h.
[55] G. Jeschke, V. Chechik, P. Ionita, A. Godt, H. Zimmermann, J. Banham, C. R. Timmel, D. Hilger, H. Jung, DeerAnalysis2006—a comprehensive software package for analyzing pulsed ELDOR data, Appl. Magn. Reson. 30 (3) (2006) 473–498, https://doi.org/10.1007/BF03166213.
[56] S.G. Worswick, J.A. Spencer, G. Jeschke, I. Kuprov, Deep neural network processing of DEER data, Sci. Adv. 4 (8) (2018) eaat5218, https://doi.org/10.1126/sciadv.aat5218.
[57] J. Keeley, T. Choudhury, L. Galazzo, E. Bordignon, A. Feintuch, D. Goldfarb, H. Russell, M.J. Taylor, J.E. Lovett, A. Eggeling, et al., Neural networks in pulsed dipolar spectroscopy: a practical guide, J. Magn. Reson. 338 (2022) 107186, https://doi.org/10.1016/j.jmr.2022.107186.
[58] O. Schiemann, C.A. Heubach, D. Abdullin, K. Ackermann, M. Azarkh, E. G. Bagryanskaya, M. Drescher, B. Endeward, J.H. Freed, L. Galazzo, et al., Benchmark test and guidelines for DEER/PELDOR experiments on Nitroxide-labeled biomolecules, J. Am. Chem. Soc. 143 (43) (2021) 17875–17890, https://doi.org/10.1021/jacs.1c07371.
[59] F. Neese, The ORCA program system, WIREs Comput. Mol. Sci. 2 (1) (2012) 73–78, https://doi.org/10.1002/wcms.81.
[60] A.K. Rappe, C.J. Casewit, K.S. Colwell, W.I.I.I. Goddard, W.M. Skiff, Uff, a full periodic-table force-field for molecular mechanics and molecular-dynamics simulations, J. Am. Chem. Soc. 114 (25) (1992) 10024–10035, https://doi.org/10.1021/ja00051a040.
[61] E.A. Suturina, D. Häussinger, K. Zimmermann, L. Garbuio, M. Yulikov, G. Jeschke, I. Kuprov, Model-free extraction of spin label position distributions from pseudocontact shift data, Chem. Sci. 8 (4) (2017) 2751–2757, https://doi.org/10.1039/c6sc03736d.
[62] G. Tesei, J.M. Martins, M.B.A. Kunze, Y. Wang, R. Crehuet, K. Lindorff-Larsen, DEER-PREdict: software for efficient calculation of spin-labeling EPR and NMR data from conformational ensembles, PLoS Comput. Biol. 17 (1) (2021) e1008551, https://doi.org/10.1371/journal.pcbi.1008551.
[63] G. Jeschke, Ensemble models of proteins and protein domains based on distance distribution restraints, Proteins 84 (4) (2016) 544–560, https://doi.org/10.1002/prot.25000.
[64] D. Gendreizig, A. Kalarikkal, S.L. Holtbrugge, S. Mukherjee, L. Galazzo, S. Kucher, A. Rosspeintner, L.V. Schafer, E. Bordignon, A combined approach to extract rotational dynamics of globular proteins undergoing liquid-liquid phase separation, J. Phys. Chem. B 129 (4) (2025) 1185–1196, https://doi.org/10.1021/acs.jpcb.4c06259.
[65] Y. Polyhach, E. Bordignon, R. Tschaggelar, S. Gandra, A. Godt, G. Jeschke, High sensitivity and versatility of the DEER experiment on nitroxide radical pairs at Q-band frequencies, Phys. Chem. Chem. Phys. 14 (30) (2012) 10762–10773, https://doi.org/10.1039/c2cp41520h.
[66] S. Kucher, C. Elsner, M. Safonova, S. Maffini, E. Bordignon, In-cell double Electron-Electron resonance at Nanomolar protein concentrations, J. Phys. Chem. Lett. 12 (14) (2021) 3679–3684, https://doi.org/10.1021/acs.jpclett.1c00048.